Available online at www.sciencedirect.com
ScienceDirect
Journal of Sound and Vibration 309 (2008) 167–177
JOURNAL OF SOUND AND VIBRATION
www.elsevier.com/locate/jsvi

Comparisons of predicted steady-state levels in rooms with extended- and local-reaction bounding surfaces

Murray Hodgson*, Andrew Wareing[1]

Acoustics and Noise Research Group, SOEH and MECH, University of British Columbia, 3rd Floor, 2206 East Mall, Vancouver, BC, Canada V6T 1Z3

Received 13 December 2005; received in revised form 13 March 2007; accepted 7 June 2007
Available online 12 September 2007

Abstract

A combined beam-tracing and transfer-matrix model for predicting steady-state sound-pressure levels in rooms with multilayer bounding surfaces was used to compare the effect of extended- and local-reaction surfaces, and the accuracy of the local-reaction approximation. Three rooms—an office, a corridor and a workshop—with one or more multilayer test surfaces were considered. The test surfaces were a single-glass panel, a double-drywall panel, a carpeted floor, a suspended-acoustical ceiling, a double-steel panel, and glass fibre on a hard backing. Each test surface was modeled as of extended or of local reaction. Sound-pressure levels were predicted and compared to determine the significance of the surface-reaction assumption. The main conclusions were that the difference between modeling a room surface as of extended or of local reaction is not significant when the surface is a single plate or a single layer of material (solid or porous) with a hard backing. The difference is significant when the surface consists of multilayers of solid or porous material and includes a layer of fluid with a large thickness relative to the other layers. The results are partially explained by considering the surface-reflection coefficients at the first-reflection angles.
© 2007 Elsevier Ltd. All rights reserved.

1. Introduction

In this paper, predicted steady-state sound-pressure levels in rooms with realistic bounding surfaces are discussed. Many models for predicting room acoustics are energy-based, ignore phase, and model the bounding surfaces by the (angularly invariant) energy-absorption coefficient. Wave-based models are inherently more accurate, consider phase, and describe surfaces by the (complex) normal surface impedance. The surfaces of many rooms comprise multiple layers of panels, air or poroelastic, sound-absorbing materials. The normal surface impedance varies with incident angle—that is, they are of extended reaction. However, many prediction models make the local-reaction approximation, whereby the normal surface impedance does not vary with incident angle. It is clearly important to understand the effect of this approximation on predicted steady-state levels in typical rooms with typical bounding surfaces.

*Corresponding author. Tel.: +1 603 822 3073; fax: +1 604 822 9588.
E-mail address: hodgson@mech.ubc.ca (M. Hodgson).
[1]Current address: Bombardier Aerospace, 123 Garratt Blvd, Toronto, ON, Canada M3 K 1Y5. Mail Stop: N45-32.

0022-460X/$ - see front matter © 2007 Elsevier Ltd. All rights reserved.
doi:10.1016/j.jsv.2007.06.069

While the literature contains many reports of sound-field predictions in enclosed spaces, few researchers have studied the interaction between the detailed surface acoustical characteristics and the resulting sound field. In particular, few have considered the relative effects of modeling surfaces as of local or of extended reaction and, therefore, the accuracy of the local-reaction approximation. The effects of angularly varying surface-absorption coefficients have been considered by several researchers using energy-based (e.g., ray-tracing) models [1–4]. The surface-reaction characteristics of surfaces were discussed by Attenborough [5] who pointed out that, although many have argued that the local-reaction assumption is valid for porous materials, experiment shows otherwise. Experiments performed by, for example, Klein and Cops [6] and Tamura, Allard and Lafarge [7] showed that the measured surface impedances of various porous materials vary significantly with angle of incidence. Morse [8] developed a model for predicting sound in enclosures based on the local-reaction assumption, noting that it might be inadequate. Pan and Bies [9–12] studied the interaction between room boundaries and the contained steady-state and transient sound fields theoretically and experimentally. In summary, the differences in the predicted steady-state sound field resulting from local- and extended-reaction surfaces in typical rooms remain largely unknown.

In recent research [13,14] a novel model for predicting steady-state sound-pressure levels in rooms with multilayer bounding surfaces has been developed. The model is based on combining a beam-tracing model with phase for predicting room steady-state sound fields, with a transfer-matrix model for predicting the complex acoustical characteristics of multilayer surfaces. Surfaces are nominally of extended reaction, but can be forced to be of local reaction.

In the work reported here, the new room-prediction model was applied to rooms, in order to study the effect that extended- and local-reaction room surfaces have on predicted steady-state sound-pressure levels. In particular, it was of interest to investigate the accuracy of the local-reaction approximation. Three room configurations were considered; in each, one or more of the room surfaces was defined as a multilayer test surface. Furthermore, each test surface was modeled in two ways—of extended reaction and of local reaction. An extended-reaction surface was modeled by predicting the complex surface impedance at the angle of incidence of the beam incident on the surface, as calculated by the beam-tracing algorithm. A local-reaction surface was modeled by predicting the complex surface impedance at normal incidence, pre-computed prior to beam tracing. For each room configuration, the sound-pressure level was predicted for each surface implementation. The sound-pressure levels were compared, to determine the difference between the extended- and local-reaction surface assumptions on predicted room levels.

2. Beam-tracing model

Following is a brief description of the beam-tracing model; full details are presented elsewhere [13,14]. The model was created by combining a triangular-beam-tracing room-prediction model including phase, and a transfer-matrix model to describe the room surfaces. The transfer-matrix model predicts the complex pressure-reflection coefficient of a multilayer surface as a function of frequency and incident angle. A surface comprises layers of elastic solids (i.e. panels), fluids (e.g. air) and poroelastic (e.g. sound-absorbing) materials, which are assumed isotropic and infinite in lateral extent. Elastic solids are described by plate theory; poroelastic layers are described using Biot theory. Wave propagation through each layer is described by a transfer matrix. Wave propagation throughout the complete multilayer surface is found by combining the transfer matrices of the individual layers, and interface matrices that satisfy the boundary conditions of adjacent layers, into a system transfer matrix. The acoustical properties (e.g. the pressure reflection coefficient) of the surface are found from the system transfer matrix.

The development of the beam-tracing model involved source and beam initialization, beam tracing, source–receiver-path estimation and the calculation of the sound-pressure level at the receiver. A spherical wave was approximated by a point source surrounded by an icosahedron with subdivided triangular faces. A beam was defined by the point source as the vertex, and the three vertices of an icosahedron face. Each beam was propagated through the room by tracing its centre ray up to a specified reflection order, in an attempt to find a valid source–receiver path. The beam-face represented a portion of the spherical sound wavefront as a complex pressure. With each surface reflection, the associated complex pressure-reflection coefficient, calculated by a transfer-matrix model for multilayer surfaces, was multiplied by the incident beam's complex

pressure to find the pressure at the reflected beam-front. The sum of the complex pressures at the beam-face for each occurrence of a valid source–receiver path is that beam's contribution to the sound pressure at the receiver. The sum of the pressure contributions from all beams yields the steady-state sound-pressure level at the receiver point. The model works in the frequency domain.

The transfer-matrix model was validated in the case of surfaces that are commonly found in rooms—a single-glass panel, a double-drywall panel, a carpeted floor, and a glass-fibre layer on a hard backing—by comparing predicted surface impedances and reflection coefficients to predictions by other known theories and with experiment. Very good agreement was found. The validation process for the beam-tracing model involved comparing it with an image-source model with phase, for three different room configurations. It also involved determining the reflection order and the number of beams needed to ensure accurate predictions. Considering the three rooms, with surfaces with diffuse-field surface-absorption coefficients of 0.1, and sound-pressure levels in octave bands from 63 to 2000 Hz, it was found that 1280 beams (5120 at 63 Hz) and a reflection order of 24 resulted in predicted sound-pressure levels converging within 0.5 dB.

3. Test configurations

Three room configurations, representing a small, empty office, a corridor, and a small, empty industrial workshop, were studied. Details of the room geometries are given in Table 1 and Fig. 1. Room 1 (the office) had length equal to width equal to height. Room 2 (the corridor) had length greater than height and width. Room 3 (the workshop) had height less than length and width.

The test surfaces considered in the work were a single-glass panel, a double-drywall panel, a carpeted floor, a suspended-acoustical ceiling, a double-steel panel, and a glass-fibre layer on a hard backing. All surfaces, with the exception of the double-steel panel and the suspended-acoustical ceiling, had been involved in the previous transfer-matrix-model validation [13,14]. The material properties of the glass and drywall (gypsum board) are given in Table 2; the properties of the carpet and glass-fibre porous layers are given in Table 3 [15,16]. The material properties of the steel plate are given in Table 4. The suspended-acoustical ceiling consisted of two layers with a rigid (e.g. concrete) backing; the first layer was a 12-mm-thick layer of the glass

Table 1
Room and multilayer-surface configurations involved in the predictions

Room no.	Test surface	Location of test surface	Dimensions $[L \times W \times H]$ (m)	Source position $\{S_x, S_y, S_z\}$	Receiver position $\{R_x, R_y, R_z\}$
1	Single-glass panel	Wall at $y = 0$	$[3 \times 3 \times 3]$	{0.5, 1.5, 2.0}	{2.5, 1.5, 1.8}
	Double-drywall panels	Walls, $x = 0$, $x = 3$, $y = 0$, and $y = 3$			
	Carpeted floor	Floor at $z = 0$			
	Suspended-acoustical ceiling	Ceiling at $z = 3$			
2	Single-glass panel	Wall at $y = 0$	$[10 \times 3 \times 3]$	{0.5, 1.5, 2.0}	{9.5, 1.5, 1.8}
	Double-drywall panels	Walls, $x = 0$, $x = 10$, $y = 0$, and $y = 3$			
	Carpeted floor	Floor at $z = 0$			
	Suspended-acoustical ceiling	Ceiling at $z = 3$			
3	Single-glass panel	Wall at $y = 0$	$[10 \times 10 \times 3]$	{0.5, 5.0, 1.5}	{9.5, 5.0, 1.8}
	Double-steel panels	Walls, $x = 0$, $x = 10$, $y = 0$, and $y = 10$			
	Double-steel panel	Ceiling at $z = 3$			
	Glass fibre on hard backing	Ceiling at $z = 3$			

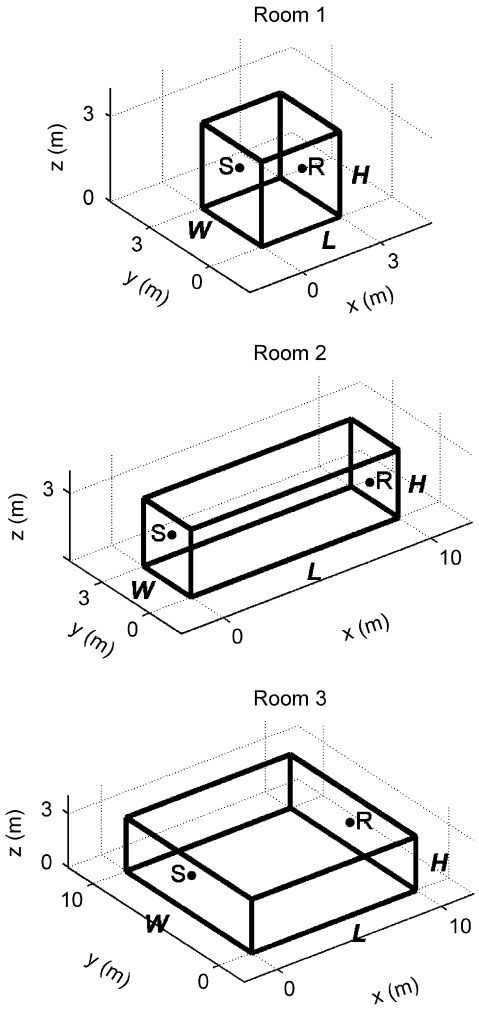

Fig. 1. Three test-room configurations, showing dimensions and source and receiver positions.

Table 2
Material properties of the glass and drywall plates involved in the predictions

Material	Glass	Drywall (gypsum board)
Thickness (mm)	6.0	12.0
Density (kg/m^3)	2500.0	1200.0
Young's modulus (GPa)	60.0	7.0
The Poisson ratio	0.33	0.25

fibre described in Table 3, the second layer was a 457-mm-thick air gap. An average diffuse-field absorption coefficient of 0.1, invariant with incident angle or frequency, was assigned to all non-multilayer test surfaces. The test surfaces were chosen as relevant to the three types of rooms. The glass panel was assigned to one wall in each of the rooms to model a large window (configurations G1, G2, and G3). The double-drywall panel modeled the four walls in rooms 1 and 2 (D1, D2). Double-steel panels were used to model the walls in room 3 (SW3), because an industrial workshop is commonly constructed with metal cladding. Carpet on a hard backing was used as the floor surface in rooms 1 and 2 (C1, C2). It is very common for offices and corridors to have acoustical tiles suspended from a concrete ceiling; thus, the suspended-acoustical ceiling was included in

Table 3
Material properties of the porous layers used in prediction [15,16]

Material property	Glass fibre [15]	Carpet [16]	
	Layer 1	Layer 1	Layer 2
Thickness (mm)	100.0	3.5	3.5
Frame density (kg/m^3)	130.0	60.0	60.0
Frame shear modulus (MPa)	$(2200+j)\times10^{-3}$	$(10+j5)\times10^{-3}$	$(10+j5)\times10^{-3}$
The Poisson ratio	0	0	0
Flow resistivity (N s/m^4)	40,000	20,000	5000
Porosity	0.94	0.99	0.99
Tortuosity	1.06	1.00	1.00
Viscous dimension (m)	0.56×10^{-4}	1.5×10^{-4}	2.3×10^{-4}
Thermal dimension (m)	1.12×10^{-4}	2.2×10^{-4}	2.8×10^{-4}

Both layers had a rigid backing; the carpet consisted of two porous layers. The properties of the air-saturated pores of all porous materials were as follows: air density = 1.2 kg/m^3, sound speed = 344 m/s, standard air pressure = 101.3 kPa, dynamic viscosity = 18.2×10^{-6} N s/m^2, specific heat ratio = 1.4, and Prandtl number = 0.710.

Table 4
Material properties of the steel plate involved in the predictions

Material	Steel
Thickness (mm)	1.6
Density (kg/m^3)	2500.0
Young's modulus (GPa)	210.0
The Poisson ratio	0.33

rooms 1 and 2 (SAC1, SAC2). Two types of test surfaces were applied to the ceiling in room 3. A common ceiling in a workshop is made of metal paneling, or concrete that is treated acoustically (or thermally) with porous, sound-absorbing material. The first ceiling type was approximated by the double-steel panels used as the walls in room 3 (SC3). The second type was modeled by a 100-mm glass-fibre layer with a rigid backing (FG3).

All tests were performed with the same set of prediction parameters, as follows: constant source sound-power level of 80 dB at each frequency; 3920 beams emitted by the source; reflection order of 50; frequency range of 50–4000 with 10 Hz increments; source positioned at 0.5 m in front of, and at the centre of, the wall at $x = 0$ (see Fig. 1), and at a constant height of 2 m; receiver positioned at 0.5 m in front of, and at the centre of, the wall at $x = L$ (see Fig. 1), and at a constant height of 1.8 m. While results may vary with receiver position, only one position in each room is discussed here. The numbers of beams and reflections were chosen to ensure that predicted levels were generally accurate to within about 0.5 dB. At 63 Hz, the number of beams was chosen to be lower than the optimal value of 5120 identified in previous validation tests [13], to obtain reasonable runtimes, and following further validation tests on the new test configurations. Calculation times on a Pentium PC with 133 MHz CPU and 128 MB RAM were typically 18–24 h for the extended-reaction cases, and 0.5–1 h for the local-reaction cases.

4. Results and discussion

Table 5 contains a summary of the octave-band and total levels for all test configurations in both the extended and local-reaction cases, and the differences between the local- and extended-reaction levels (the '*L*–*E* difference').

A few comments generally applicable to all results are in order. Given that individual predicted levels are assumed to be accurate to within 0.5 dB, differences in level of less than 1 dB will not be considered significant

Table 5
Predicted octave-band and total steady-state levels for all test configurations

Config.	Surface/room	Reaction	Octave band (Hz)						
			63	125	250	500	1000	2000	Total
G1	Glass/room 1	Extended	88.1	95.3	95.9	102.0	104.2	107.8	112.5
		Local	89.0	95.4	95.9	102.0	104.2	107.9	112.6
		L–E	0.9	0.1	0.0	0.0	0.0	0.1	0.1
G2	Glass/room 2	Extended	85.0	89.2	88.3	93.5	99.7	102.5	106.6
		Local	85.1	89.3	88.4	93.5	99.7	102.6	106.7
		L–E	0.1	0.1	0.1	0.0	0.0	0.1	0.0
G3	Glass/room 3	Extended	86.9	81.2	86.4	91.4	94.7	98.5	102.7
		Local	86.9	81.3	86.4	91.4	94.8	98.5	102.7
		L–E	0.1	0.0	0.0	0.0	0.0	0.0	0.0
D1	Drywall/room 1	Extended	86.7	97.7	98.9	104.4	107.0	110.5	115.1
		Local	81.6	99.5	98.8	104.9	107.0	110.8	115.3
		L–E	−5.2	1.9	−0.1	0.5	0.0	0.4	0.2
D2	Drywall/room 2	Extended	83.8	91.6	91.9	96.5	101.6	104.6	108.7
		Local	86.1	92.4	92.6	96.0	101.8	104.7	108.8
		L–E	2.4	0.7	0.7	−0.4	0.1	0.0	0.1
C1	Carpet/room 1	Extended	85.8	94.5	96.5	100.6	103.0	105.3	110.2
		Local	85.8	94.6	96.8	101.1	104.1	106.9	111.7
		L–E	0.0	0.0	0.3	0.6	1.1	1.6	1.5
C2	Carpet/room 2	Extended	85.5	85.0	82.8	89.2	95.2	98.0	101.9
		Local	70.1	80.6	83.7	92.6	95.6	98.2	102.4
		L–E	−15.4	−4.4	0.9	3.4	0.4	−0.2	0.5
SAC1	SAC/room 1	Extended	86.5	90.6	90.4	97.3	101.3	104.3	108.3
		Local	79.3	88.9	91.6	98.0	101.1	104.2	108.3
		L–E	−7.2	−1.7	1.3	0.7	−0.2	−0.1	0.0
SAC2	SAC/room 2	Extended	84.9	83.9	80.4	89.2	94.4	98.0	101.9
		Local	72.6	79.5	82.3	91.6	95.2	98.0	102.0
		L–E	−12.3	−4.4	1.9	2.4	0.8	−0.1	0.1
SW3	Steel walls/room3	Extended	85.5	83.0	88.0	93.1	96.1	100.0	104.1
		Local	85.0	78.3	90.1	93.5	96.1	100.0	104.3
		L–E	−0.5	−4.7	2.0	0.4	0.0	0.0	0.1
SC3	Steel ceiling/room 3	Extended	86.9	81.7	90.1	92.0	95.5	99.7	103.8
		Local	86.9	79.8	88.4	93.1	95.9	99.9	104.0
		L–E	0.1	−1.9	−1.8	1.1	0.4	0.1	0.2
FG3	FG ceiling/room 3	Extended	80.7	74.4	75.4	86.3	89.8	93.8	97.7
		Local	80.7	74.4	75.5	87.4	89.9	94.0	97.9
		L–E	0.0	0.0	0.1	1.1	0.1	0.2	0.3

in the discussion below. In addition, octave-band levels tend to increase with frequency, because the source had constant power output per frequency and octave bands have greater bandwidths at high frequency; all else being equal, levels increase by 3 dB per octave band. Finally, levels at high frequency in a given room with different non-absorptive surfaces (e.g., a glass panel or double-drywall panels) would be expected to be very similar. However, Table 5 shows 2-kHz levels in rooms 1 or 2 which are 2–3 dB higher with four double-drywall walls than with a single glass-panel wall. This apparently anomalous result is explained by the fact that non-multilayer surfaces were assumed to have absorption coefficients of 0.1, which is more absorbent than the non-absorptive multilayer test surfaces at high frequency.

For some, but not all, of the test configurations and frequencies there were significant *L–E* differences. Consideration of the reflection coefficients of the test surfaces may provide a partial explanation of these results. Thus, two sets of reflection coefficients were calculated for each surface—one from the extended-reaction surface impedance, and the other from the local-reaction surface impedance. The two impedances were calculated using the transfer-matrix model, and the corresponding reflection coefficients obtained (using Eq. (2) in Ref. [12]). The reflection coefficients of each of the test surfaces were calculated at the centre

frequencies of the 63- to 2000-Hz octave bands, for angles of 0–90°, with 1° increments. Detailed results are only presented here for the case of the suspended-acoustical ceiling (see Fig. 4); full results are given in Ref. [13].

In addition to the reflection-coefficient information, knowledge of the incident angles associated with the various reflection paths is required. Besides the direct sound, the largest contributions to the sound pressure at the receiver are expected to be from first-order reflections. Given the reflection coefficients predicted for the applicable incident angle, the influence of the test surface on the sound pressure at the receiver can be estimated from the incident angle of the first-order-reflection paths. Then, the L–E differences may, at least partially, be explained by the differences between the extended- and local-reaction coefficients at the angles of incidence of the first-order-reflection paths. The incident angles of the first-order reflected-sound paths for all three rooms are presented in Table 6.

It is important to note that L–E differences may also be caused by interference effects. The magnitude and phase of the acoustical pressure are determined for both the direct beam and the beam reflected at a boundary. The calculated complex reflection coefficient may be different for the extended- and local-reacting reflecting surfaces. The total pressure at a receiver point, resulting from the summation of the direct and reflected pressures, may yield higher or lower levels due to constructive or destructive interference.

The detailed results for the suspended-acoustical ceiling in room 2 (SAC2) are shown in Figs. 2 and 3, and in Table 5. The largest L–E differences were observed in these test configurations. In the narrow-band results, significant L–E differences are seen. At low frequency, levels were much lower in both rooms with the test surface modeled as of local reaction. In rooms 1 and 2 at 63 Hz, octave-band local-reaction levels were 7.2 and 15.4 dB lower than the extended-reaction levels, respectively. At 125 Hz, they were 1.7 and 4.4 dB lower. At 250 Hz, the local-reaction levels were higher by 1.3 and 0.9 dB. At 500 Hz, in room 2, the local-reaction level was higher by 3.4 dB. The levels were similar at this frequency in room 1, and at 1000 and 2000 Hz in both rooms. The extended- and local-reaction reflection coefficients for this test surface are shown in Fig. 4. It is not surprising, given the room-prediction results, that the two reflection coefficients are very different in both their real and imaginary parts at all frequencies. The greatest difference in the room-prediction results occurs at low frequency, particularly in the 63-Hz octave band for which the extended-reaction levels were higher by 7.2 and 15.4 dB in rooms 1 and 2, respectively. At 63 Hz, the real part of the extended-reaction coefficient is much greater than the real part of the local-reaction coefficient at all angles except normal incidence, at which the coefficients are the same. The imaginary part of the extended-reaction coefficient is greater up to an angle of 80°, at which it reaches a maximum and decreases toward −1 with increasing angle, whereas the local-reaction coefficient continues to increase toward 0 with increasing angle. The extended-reaction level was also higher in the 125- and 250-Hz octave bands; this is consistent with the larger magnitude of the extended-reaction coefficient at these frequencies. At higher frequency, the extended-reaction coefficient fluctuates in its variation with incident angle. The local-reaction coefficient varies as a smooth, monotonic curve with increasing incident angle; it follows the minima of the real part of the extended-reaction coefficient at 500–2000 Hz, and follows the maxima of the imaginary part of the extended-reaction curve at 1000 Hz. The local-reaction levels were equal to, or slightly higher than, the extended-reaction levels in both rooms at high frequency. It is difficult to relate the difference in levels in the higher frequency bands to the reflection coefficients at the first-reflection angle of incidence with the floor, which are 27.3° and 67.1° for rooms 1 and 2, respectively. At these angles, the local-reaction coefficients appear to be slightly greater in magnitude than the extended-reaction coefficients at frequencies from 500 to 2000 Hz. This is consistent with the slightly higher local-reaction levels at higher frequency in both rooms. However, differences in levels due to interference effects should not be

Table 6
Incident angles of the first-order-reflected-sound paths for the three rooms

Room	$\theta_{ceiling}$ (deg)	θ_{floor} (deg)	θ_{wall} (deg)
1 (office)	42.3	27.8	33.7
2 (corridor)	76.3	67.1	71.6
3 (workshop)	76.3	67.1	42.0

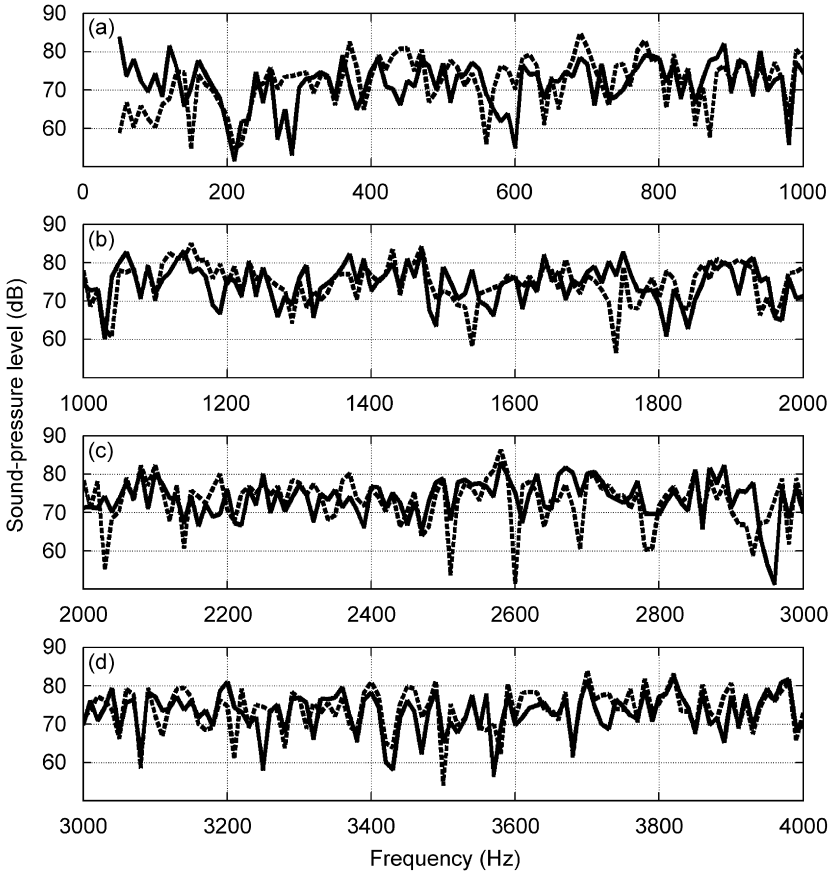

Fig. 2. Narrow-band frequency response of the steady-state sound-pressure level predicted in room 2 with a suspended acoustical ceiling; all other surfaces have an average absorption coefficient of 0.1: (——) extended reaction; (·····) local reaction: (a) 0–1000; (b) 1000–2000; (c) 2000–3000; and (d) 3000–4000 Hz.

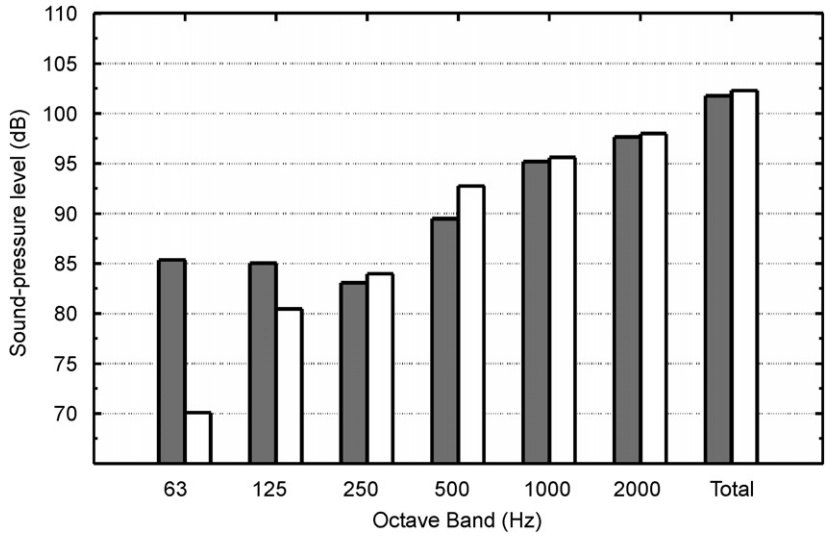

Fig. 3. Octave-band frequency response of the steady-state sound-pressure level predicted in room 2 with suspended-acoustical ceiling; all other surfaces have an average absorption coefficient of 0.1: (▓) extended reaction; (□) local reaction.

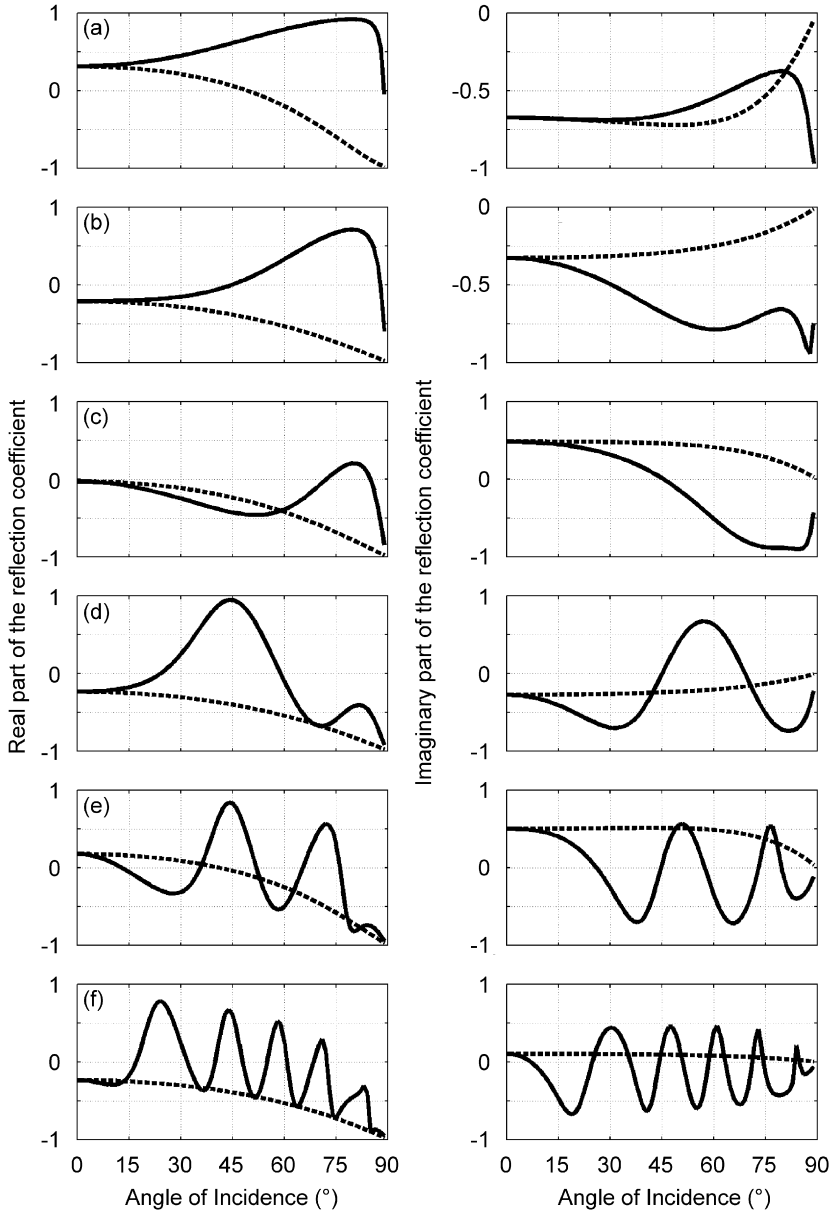

Fig. 4. Real (left) and imaginary (right) parts of the reflection coefficient of the suspended-acoustical ceiling, predicted as a function of incident angle. (——) Extended reaction; (·····) local reaction: (a) 63; (b) 125; (c) 250; (d) 500; (e) 1000; and (f) 2000 Hz.

ignored. Furthermore, the extended-reaction coefficient appears very different at individual frequencies; the comparison of single-frequency reflection coefficients in this case is difficult to relate to the octave-band-level results. There is an air gap of significant thickness in this test surface. Since the local-reaction assumption for air is known to be invalid, it is not surprising that the extended- and local-reaction coefficients are very different. Except in the case of an incident wave at normal incidence, waves transmitted through a fluid layer occur at some angle θ, for which the impedance is $Z_c/\cos(\theta)$. It is quite possible, depending on the angle, that the impedance is very different from the impedance at normal incidence, Z_c. Therefore, modeling this surface as of extended reaction is necessary in predicting the sound-pressure level in a room, due to the presence of the air gap.

Following is a summary of the main results and their implications for the other test configurations:

- G1, G2, and G3: octave-band $L-E$ differences were less than 1 dB;
- FG3: octave-band $L-E$ differences were less than 1 dB. The glass fibre used here was the same as that in the suspended acoustical ceilings, for which there were significant $L-E$ differences at lower frequencies. Here, however, the material was much thicker and there was no air gap beyond the glass-fibre layer. This suggests that the material thickness in porous layers is not a significant factor affecting the $L-E$ difference. However, it appears that the existence of a large air-gap is significant;
- C1 and C2: As might be expected for porous-absorber layers, $L-E$ differences only occurred at high frequencies, for which local-reaction levels were highest by up to 2.5 dB. The magnitude of the extended-reaction reflection coefficient was greater, and it was expected that the extended-reaction levels would be highest. As they were not, it must be that interference effects were responsible for the results;
- D1 and D2: these two configurations showed significant $L-E$ differences only at the lowest frequencies, similar to the results for SAC1 and 2. The result for room 2 was unexpected; the first-reflection angles of incidence on the walls indicated that local-reaction levels should be equal to or greater than extended-reaction levels. As this is not the case, especially at low frequency, the $L-E$ difference is likely due to phase differences between the extended- and local-reaction coefficients. The extended- and local-reaction levels are almost equal at high frequency, where phase is less of an issue;
- SC3, SW3: these configurations had similar results, with significant $L-E$ differences in the 125 and 250 Hz bands only. However, at 250 Hz the SC3 levels were highest with extended reaction, whereas in SW3 local-reaction levels were highest. This suggests that the positioning of the extended-reaction test surface, and the source–receiver position, influence predicted levels.

5. Conclusion

A novel combined beam-tracing and transfer-matrix room-prediction model has been applied to three rooms with various multilayer surfaces, and steady-state sound-pressure levels predicted assuming either local or extended reaction. The results provide insights into the differences in predicting sound-pressure levels in rooms with surfaces modeled as of extended or of local reaction, and into the accuracy of the local-reaction approximation. The following summary remarks can be made:

1. The difference between modeling a room surface as of extended or local reaction is not significant when the surface is a single plate, or a single layer of material (solid or porous) with a rigid backing. In the case of a porous layer on a rigid backing, the results likely depend on the flow resistivity of the porous layer;
2. The difference between modeling a room surface as extended or local reaction is significant when the surface consists of multilayers of solid or porous material, and includes a layer of air with a thickness that is large relative to the other layers. The local-reaction approximation can result in octave-band levels being either under- or over-estimated, by over 10 dB in some cases;
3. For surfaces for which the reflection coefficient is different when obtained using extended- and local-reaction surface impedances, the difference between the extended- and local-reaction levels may be significant, depending on the source and receiver positions. This becomes important when the positions are such that the first-reflection angle of incidence on the room surfaces is near grazing.

References

[1] H. Kuttruff, On the angular dependence of the sound absorption coefficient on the reverberation time, *Acustica* 42 (1979) 187–188 (in German).

[2] G. Benedetto, R. Spagnolo, Reverberation time in enclosures: the surface reflection law and the dependence of the absorption coefficient on the angle of incidence, *Journal of the Acoustical Society of America* 77 (4) (1985) 1447–1451.

[3] M. Hodgson, On the prediction of sound fields in large empty rooms, *Journal of the Acoustical Society of America* 84 (1) (1988) 253–261.

[4] L. Nijs, G. Jansens, G. Vermeir, M. van der Voorden, Absorbing surfaces in ray-tracing programs for coupled spaces, *Applied Acoustics* 63 (6) (2002) 611–626.
[5] K. Attenborough, Acoustical characteristics of porous materials, *Physics Reports* 82 (3) (1982) 179–227.
[6] C. Klein, A. Cops, Angle dependence of the impedance of a porous layer, *Acustica* 44 (1980) 258–264.
[7] M. Tamura, J.-F. Allard, D. Lafarge, Spatial Fourier-transform method for measuring reflection coefficients at oblique incidence. II. Experimental results, *Journal of the Acoustical Society of America* 97 (1995) 2255–2262.
[8] P.M. Morse, Some aspects of the theory of room acoustics, *Journal of the Acoustical Society of America* 11 (1939) 56–66.
[9] J. Pan, D.A. Bies, An experimental investigation into the interaction between a sound field and its boundaries, *Journal of the Acoustical Society of America* 83 (1988) 1436–1444.
[10] J. Pan, D.A. Bies, The effect of fluid–structural coupling on sound waves in an enclosure—theoretical part, *Journal of the Acoustical Society of America* 87 (2) (1990) 691–707.
[11] J. Pan, D.A. Bies, The effect of fluid–structural coupling on sound waves in an enclosure—experimental part, *Journal of the Acoustical Society of America* 87 (2) (1990) 708–717.
[12] J. Pan, D.A. Bies, The effect of fluid–structural coupling on acoustical decays in a reverberation room in the high-frequency range, *Journal of the Acoustical Society of America* 87 (2) (1990) 718–727.
[13] A. Wareing, Acoustic Modeling of Rooms with Extended-reaction Surfaces, MSc Thesis, Department of Mechanical Engineering University of British Columbia, 2000.
[14] A. Wareing, M.R. Hodgson, Beam-tracing model for predicting sound in rooms with multilayer bounding surfaces, *Journal of the Acoustical Society of America* 118 (4) (2005) 2321–2331.
[15] J.F. Allard, *Propagation of Sound in Porous Media*, Elsevier, London, 1993, p. 133.
[16] B. Brouard, D. Lafarge, J.F. Allard, Measuring and prediction of the surface impedance of a resonant sound absorbing structure, *Acta Acustica* 2 (1994) 301–306.